Zhi Li, Stavros A. Argyropoulos*

Determination of Thermal Conductivity of Mn-Al Powder Compacts using An Inverse Heat Transfer Procedure

Abstract: The effective thermal conductivities of various Mn-Al powder compact compositions were measured using an Inverse Heat Transfer Procedure, and extensive validation work was also carried out. Specially fabricated cylindrical compact specimens were used equipped with two thermocouples at strategic locations. The porosity of these specimens was also measured.

The estimated effective thermal conductivities of various Mn-Al compacts were in the range of 5.5 to 10.5 W m^{-1} $°C^{-1}$, which are much lower than that of Al (237 W m^{-1} $°C^{-1}$), and close to that of Mn (7.8 W m^{-1} $°C^{-1}$). The effective thermal conductivities of Mn-Al powder compacts decreased with an increase in the compact's Mn composition and porosity. Within the examined temperature range of 250 to 600 °C, the effect of temperature on the effective thermal conductivity was minimal. A purely theoretically derived prediction of Mn-Al compact thermal conductivity is substantially higher than the estimates of using the IHTP.

Keywords: thermal conductivity, Mn-Al powder, Inverse Heat Transfer Procedure

PACS® (2010). 65.40.-b, 81.70.-q

Zhi Li: Postdoctoral Fellow, Department of Materials Science & Engineering, University of Toronto, 184 College Street, Toronto, Ontario, CANADA M5S3E4

***Corresponding author: Stavros A. Argyropoulos:** Professor, Department of Materials Science & Engineering, University of Toronto, 184 College Street, Toronto, Ontario, CANADA M5S3E4
E-mail: stavros.argyropoulos@utoronto.ca

1 Introduction

The effective thermal conductivity of metal powder compacts is a very important property in a wide range of areas such as the assimilation of metal powder compacts in liquid metals, powder metallurgy, and reaction synthesis. Given its importance, it is not surprising that the Brailsford and Major model [1] has been proposed to estimate the theoretical effective thermal conductivities of Mn-Al compacts. Despite the potential usefulness of such an approach, however, it is not possible to incorporate into a theoretical model the numerous factors that can affect the effective thermal conductivity of powder compacts. Some of the relevant factors that have been proposed include powder size and distribution, mass fraction of component, material purity, powder surface condition, powder shape, mixing condition, and deformation of powders during compaction [2]. As such, using a theoretical model to estimate thermal conductivities of Mn-Al compacts may lead to compromised accuracy. Experimental research studies [2–6] have measured the effective thermal conductivities of various powder compacts using the laser flash method and the guarded hot plate technique [7]. However, even such experimental studies may continue to have difficulty incorporating the impact of porosity into the investigation.

The current paper, in essence, adopted a hybrid approach between the direct experimental design and the completely theoretical estimation in determining the effective thermal conductivity of Mn-Al compacts. In so doing, it was possible to take into consideration the chemical composition and porosity of the compacts. Thermal conductivities were estimated through an indirect method, using the Inverse Heat Transfer Procedure (IHTP), which utilized the experimental methodology developed by the present investigators in working with Mn-Al compacts [8–9]. Finally, the projected estimates of the thermal conductivities were calculated using the Brailsford and Major model, thereby providing a direct comparison between the estimates using this purely theoretical model with those using the proposed IHTP.

2 Experimental

Cylindrical powder compacts consisting of Mn and Al powders with different compositions were manufactured. The procedural details as well as the powder characteristics in manufacturing these compacts are outlined in previous publications [8, 9] and as such, they will not be

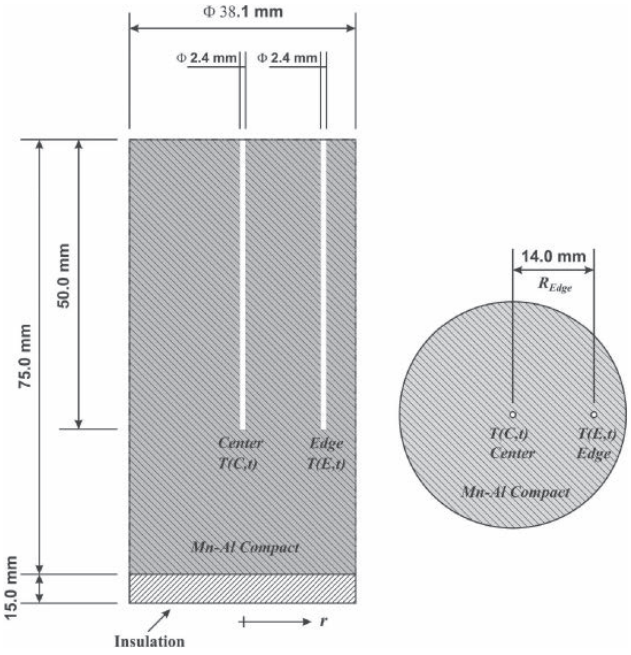

Fig. 1: Dimensional details of manufactured Mn-Al cylindrical compact specimens.

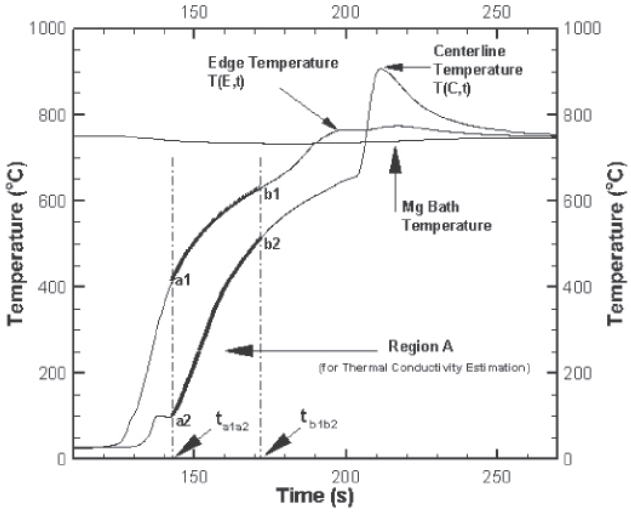

Fig. 2: Typical experimental result of a 60wt%Mn-40wt%Al cylindrical compact where the IHTP used.

described in this paper. In each cylindrical compact, two wells were drilled one in the center and the other somewhere close to the surface, and a fine thermocouple was inserted into each well. The hot junction of each thermocouple was located at the bottom of the well. Figure 1 displays various details of manufactured cylindrical compacts. At the bottom of each compact a thermal insulation material was applied [8].

These compacts, initially at room temperature, were immersed into a Mg bath at 750 °C. The size and the various details of the crucible used to melt the Mg are given in reference [8]. The temperature histories at the center and at the edge of the cylindrical compact specimens were recorded with a data acquisition system every 200 ms.

Throughout this paper the symbols $T(C, t)$ and $T(E, t)$ indicate measured temperatures at the center and at the edge of the cylindrical compact, respectively. In addition, the term "set of measurements" is used. This term denotes the two temperatures recorded, edge and centerline, every 200 ms.

For the duration of this experiment, the heat transfer from the Mg bath to the cylinder was essentially one-dimensional (i.e., radial heat transfer) since the other possible heat transfer component through the bottom of the cylinder, was rendered negligible due to the applied thermal insulation. A more detailed explanation of this aspect is given in section 4 of this manuscript.

3 Inverse heat transfer procedure (IHTP)

Figure 2 shows a typical experimental result used in the IHTP, whereby the temperature histories of the liquid Mg, compact edge $T(E, t)$ and compact centerline $T(C, t)$ are displayed. In particular, only the monotonous bolded segments $(a1, b1)$ and $(a2, b2)$ of $T(E, t)$ and $T(C, t)$ respectively, shown in region A, were used in the IHTP. In Figure 2, t_{a1a2} indicates the beginning of IHTP and t_{b1b2} denotes the time at which the IHTP finished. The plateau on the $T(C, t)$ which exists before t_{a1a2} was due to vaporization of compact moisture. In the time region from t_{a1a2} to t_{b1b2} the compact was heated only from the Mg bath, and no exothermic intermetallic reactions were observed [8, 9]. It should be pointed out these highly exothermic reactions started well after t_{b1b2} [8, 9].

Density and heat capacity data of various compact compositions are important parameters in the IHTP. The procedural details in deriving density data are outlined in great detail in reference [8]. The heat capacity data were calculated using the Neumann-Kopp rule [10]. Table 1 lists density and heat capacity data used in the IHTP.

In the IHTP developed, the measured compact edge temperature, $T(E, t)$, was used as the thermal boundary condition, and the measured compact centerline temperature, $T(C, t)$, was used as the reference temperature. The equations describing the heat transfer problem are given as follows:

Compact Type	Apparent Density (kg m^{-3}) [8]	Apparent Heat Capacity (J kg^{-1} °C^{-1}) [8]
75wt%Mn25wt%Al	4485	584.5
60wt%Mn40wt%Al	3968	648.3
50wt%Mn50wt%Al	3679	690.9
40wt%Mn60wt%Al	3429	733.5
30wt%Mn70wt%Al	3182	776.0

Table 1: Mn-Al compact apparent densities and apparent heat capacities

$$\rho C_p \frac{\partial T}{\partial t} = k \frac{1}{r} \frac{\partial}{\partial r}\left(r \frac{\partial T}{\partial r} \right) \quad \text{in } 0 < r < R_{\text{Edge}}, \quad \text{for } t_{a1a2} < t < t_{b1b2} \tag{1}$$

$$-k \frac{\partial T}{\partial r} = 0 \quad \text{at } r = 0, \quad \text{for } t_{a1a2} < t < t_{b1b2} \tag{2}$$

$$T = T(E, t) \quad \text{at } r = R_{\text{Edge}}, \quad \text{for } t_{a1a2} < t < t_{b1b2} \tag{3}$$

$$T = T(C, t) \quad \text{in } 0 < r < R_{\text{Edge}}, \quad \text{for } t = t_{a1a2} \tag{4}$$

Equation (1) describes the unsteady state heat transfer between Edge and Center of the specimen (i.e. Figure 1). Equation (2) is boundary condition derived from the symmetry of the cylindrical specimen. Equations (3) and (4) display boundary condition and initial condition, respectively.

An implicit finite difference method was employed to discretize Equation (1) with an enmeshment setting shown in Figure 3, where Δr is the mesh size, N is the node number, V_N is the control volume of node N and A_N is the interface area between control volume N and $N+1$. It should be pointed out that since the implicit finite difference method was used, at each Δt all the temperature nodes were predicted at once. Between edge and center, 100 nodes were used. The discretized equation for node N is:

$$\rho \times c_P \times V_N \times (T_N^{P+1} - T_N^P) = k \times \Delta t \times A_{N-1} \times \frac{T_{N-1}^{P+1} - T_N^{P+1}}{\Delta r} + k \times \Delta t \times A_N \times \frac{T_{N+1}^{P+1} - T_N^{P+1}}{\Delta r} \tag{5}$$

In the above equation superscript p is used to reference the time step Δt while ρ and c_p are the density and heat capacity values respectively. The above equation is not applicable for node 1 where the following equation is applicable:

$$\rho \times c_P \times V_1 \times (T_1^{P+1} - T_1^P) = k \times \Delta t \times A_1 \times \frac{T_2^{P+1} - T_1^{P+1}}{\Delta r} \tag{6}$$

Solving and rearranging any of the above equations for T_N^{p+1} the following equation is obtained:

$$T_N^{p+1} = k \times C_{N1} + C_{N2} \tag{7}$$

In this case C_{N1} and C_{N2} are constants. Equation (7) indicates that at every time step, the temperature of every node can be presented as a linear function of thermal conductivity. Applying Equation (7) to the first node of Figure 3, the following formula is derived.

$$T_1^{p+1} = k \times C_{11} + C_{12} \tag{8}$$

As already mentioned, the goal of IHTP developed is to make the calculated compact centerline temperature T_1^{p+1} to be equal to the measured one $T(C, t)$ by estimating an effective thermal conductivity k_e.

This linear relation between the calculated temperature and the effective thermal conductivity demonstrated by Equations (7) and (8) was the foundation of the algorithm developed. This algorithm makes use of two guessed compact effective thermal conductivities k_{g1} and k_{g2}. These two guessed constants were utilized in the linear set of Equations (5). Referring to node 1, two compact centerline temperatures $T_{1,g1}^{p+1}$ and $T_{1,g2}^{p+1}$ can be obtained:

$$T_{1,g1}^{p+1} = k_{g1} \times C_{11} + C_{12} \tag{9}$$

$$T_{1,g2}^{p+1} = k_{g2} \times C_{11} + C_{12} \tag{10}$$

Solving the Equations (9) and (10) for C_{11} and C_{12} the following two equations were derived:

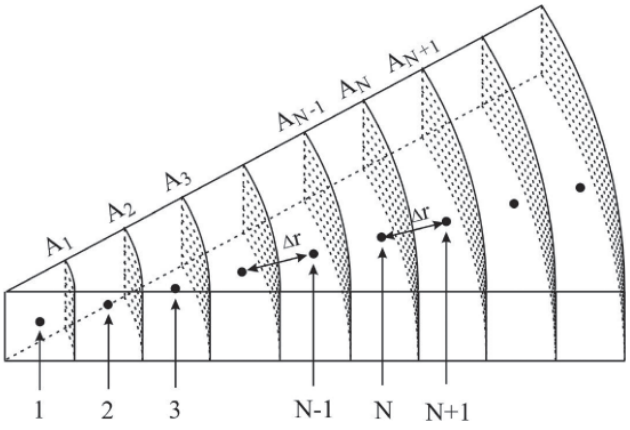

Fig. 3: An 1-D enmeshment setting for discretization of equation 1 for a unit thickness.

$$C_{11} = \frac{T_{1,g1}^{p+1} - T_{1,g2}^{p+1}}{k_{g1} - k_{g2}} \tag{11}$$

$$C_{12} = \frac{k_{g1} \times T_{1,g1}^{p+1} - k_{g2} \times T_{1,g2}^{p+1}}{k_{g1} - k_{g2}} \tag{12}$$

Substituting the measured compact centerline temperature $T(C, t^{p+1})$ and Equations (11) and (12) into Equation (8) the estimate of thermal conductivity k_e is given by:

$$k_e = \frac{T(C, t^{p+1}) \times (k_{g1} - k_{g2}) - (k_{g1} \times T_{1,g2}^{P+1} - k_{g2} \times T_{1,g1}^{P+1})}{T_{1,g1}^{P+1} - T_{1,g2}^{P+1}} \tag{13}$$

Once the estimation of the compact effective thermal conductivity is achieved the correct compact thermal field is calculated. This procedure is repeated for every set of measurements recorded. The corresponding flowchart for describing this IHTP algorithm is shown in Figure 4.

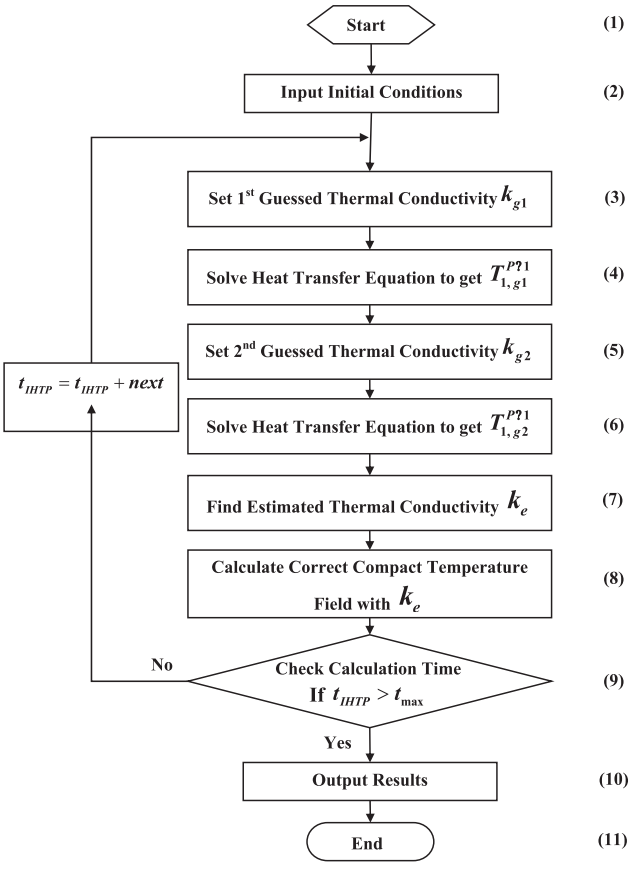

Fig. 4: IHTP flow chart for estimating effective thermal conductivities of compacts

4 Validation

Extensive validation was undertaken, focusing on three important components. (1) The impact of compact immersion on the Mg bath. (2) The influence of thermocouple holes in the compact and the insulation at the bottom of the compact shown in Figure 1. (3) The validity of IHTP that was developed. The validation work for the first and second components was carried out using a commercial computational fluid dynamics package called FLOW-3D. The thermo-physical properties used in the FLOW-3D simulation are listed in Table 2.

For the first component, an immersion procedure was simulated using the FLOW-3D to evaluate the impact of the immersion of Mn-Al compact on the flow field of the Mg bath. This procedure is described as: (1) a 25 °C Mn-Al compact with a dimension of Φ38.0 × 75.0 mm is immersed with a constant immersion velocity of 50.0 mm s^{-1} into a 750 °C Mg bath, which is shown in Figure 5 (a); (2) once the Mn-Al immersion depth reaches 63.0 mm, the compact is held motionless in the Mg bath, which is shown in Figure 5 (b). Figure 6 (a) shows the Mg bath flow pattern during the compact immersion process. It can be seen that the stronger flow region within the Mg bath is just under the Mn-Al compact. This is not surprising since this region is directly under the compact impact. Figure 6 (b) presents the change over time in the maximum velocity in the Mg bath during compact immersion. It can be seen that the velocity field induced by the compact immersion is very weak. The maximum velocity is less than 0.082 m s^{-1}. And the velocity slows down dramatically within 20 s. So, the influence of compact impact is ignored in the subsequent numerical modeling work.

For the second component, it was important to verify the heat transfer from the Mg bath to the cylindrical compact was 1-D rather than 3-D. Accordingly, utilizing the Flow-3D, a simulation of the temperature field

	Mg		Mn-Al Compact	Insulation Material
	Solid	Liquid		
Density (kg m^{-3})	1740.0	1580.0	3679.0	256.3
Heat Capacity (J kg^{-1} °C^{-1})	1350.0	1320.0	690.9	1046.7
Thermal Conductivity (W m^{-1} °C^{-1})	145.0	79.0	10.0	0.1
Latent Heat (J kg^{-1})	368000			
Viscosity (N s m^{-2})	0.0013			

Table 2: Thermo-physical properties used in FLOW-3D simulation

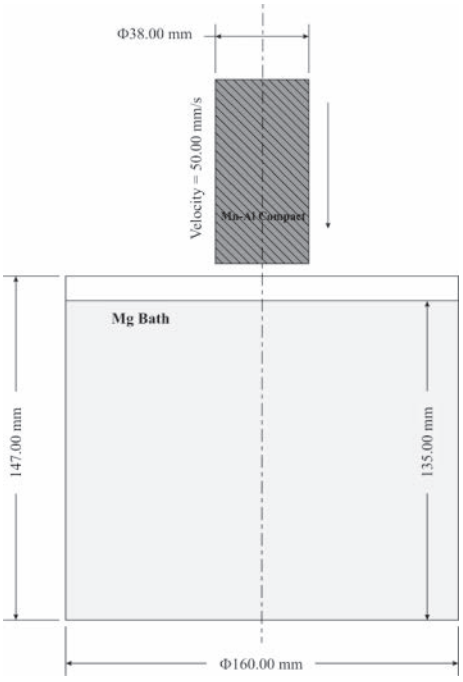

(a) Moving Compact

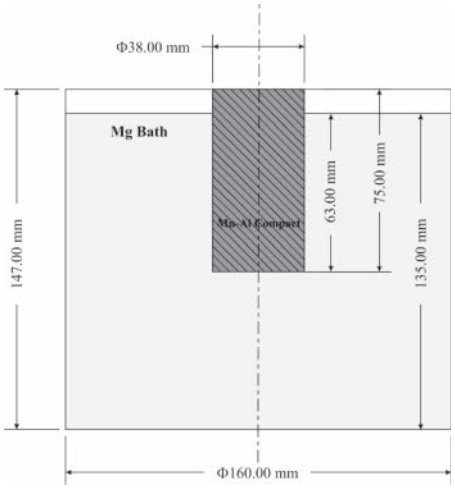

(b) Motionless compact

Fig. 5: Schematics for a Mn-Al compact immersion process into a Mg bath

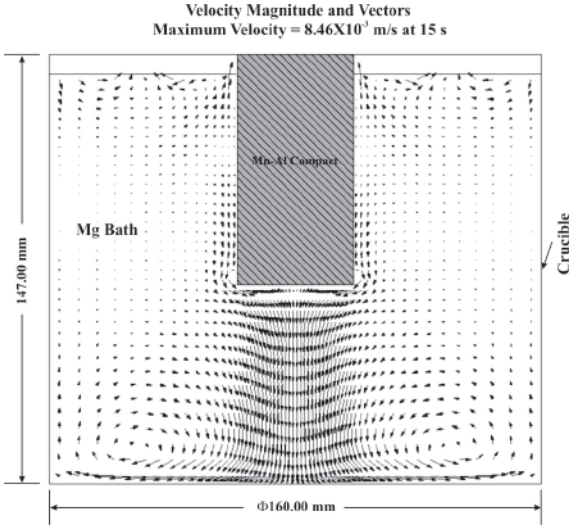

(a) Mg bath flow pattern

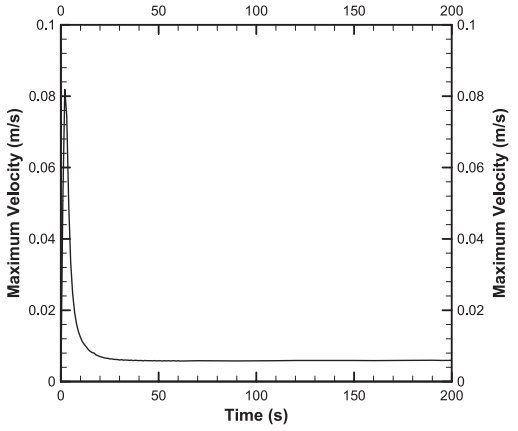

(b) Maximum velocity in Mg bath

Fig. 6: Simulation results for a Mn-Al compact immersing into Mg bath

inside the compact was carried out, using 3-D approach. In this simulation, the bottom insulation and the thermocouple holes were taken into account. Furthermore the compact was considered motionless in a 750 °C Mg bath.

Figure 7 displays the configuration of the simulation. The temperature histories for six positions inside the compact, points 11, 12, 13, 21, 22, and 23 shown in Figure 7, were calculated. It can be seen from Figure 7 that points 11, 12 and 13 are at the compact centerline, while points 21, 22 and 23 are 14 mm from the compact centerline. By associating the temperature histories among points with the same distance from the compact centerline (i.e., among points 11, 12, 13, and among points 21, 22, 23), it is possible to evaluate whether the 1-D simplification is warranted. Figures 8 and 9 display the temperature history comparisons for each set of 3 compact points shown in Figure 7. By comparing the temperature histories, it was found that the points with the same distance from the compact centerline (i.e. group of points 11, 12, 13 and group of points 21, 22, 23 of Figure 7) have very similar temperature histories. This fact implies that the compact insulation can substantially reduce the heat transfer from the bottom of the compact, and in addition, the

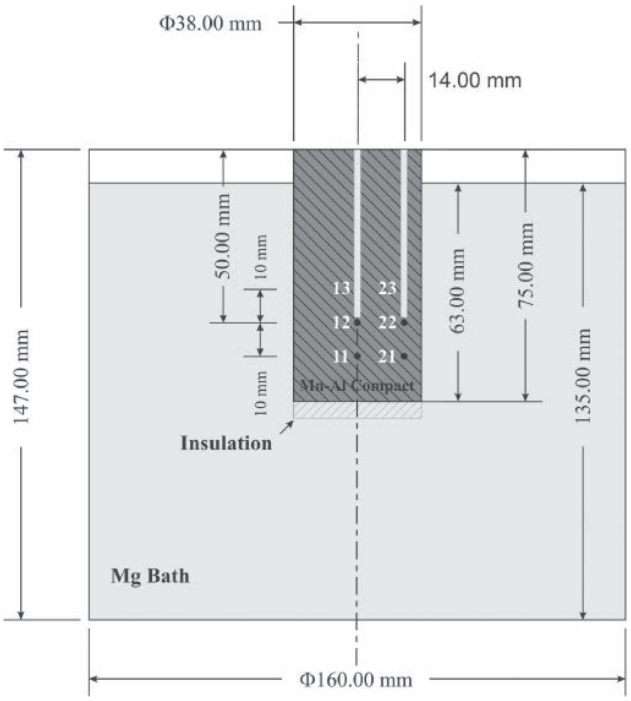

Fig. 7: Simulation configuration for a 3-D Mn-Al compact with thermocouple holes and bottom insulation immersed into a Mg bath

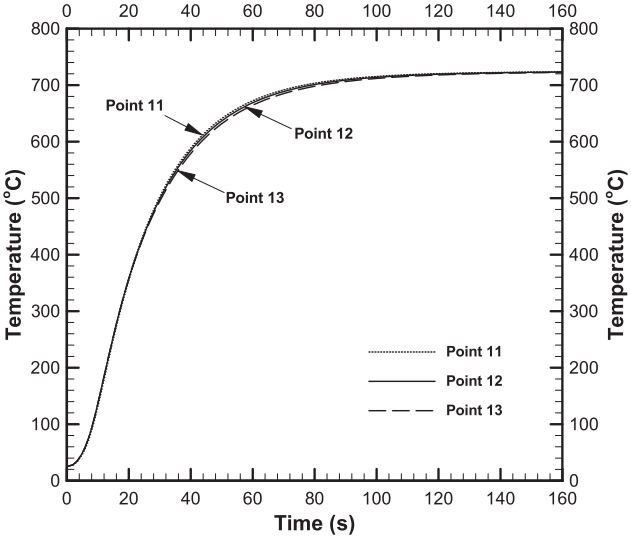

Fig. 8: Comparison for calculated temperature histories of compact points 11, 12 and 13 shown in Figure 7

thermocouple holes have only a negligible effect on the compact temperature fields. The previous analyses indicate that under the current study, the heat transfer in the compact is very close to 1-D. So, the subsequent inverse heat transfer procedure for determining the Mn-Al compact effective thermal conductivity was developed using the 1-D simplification.

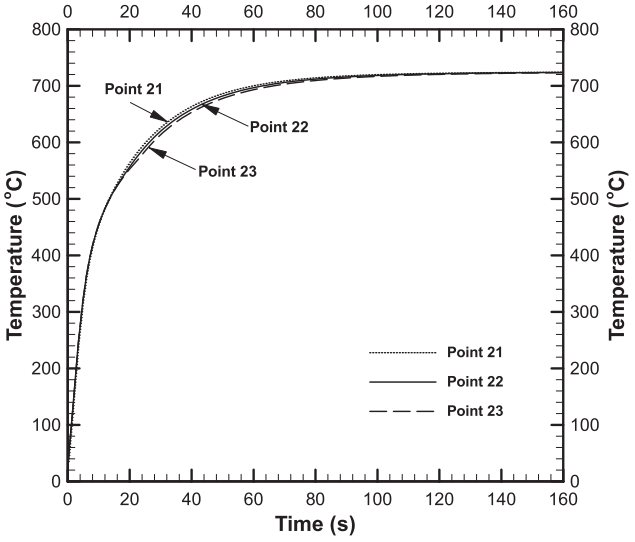

Fig. 9: Comparison for calculated temperature histories of compact points 21, 22 and 23 shown in Figure 7

For the third component, a virtual experiment was designed to test the accuracy of IHTP. This experiment was formulated by first setting a direct problem and subsequently using the results from the direct problem to solve the inverse problem. The direct problem utilizes elements of transient heat transfer of a cylinder with infinite length shown in Figure 10 (a). In this case, the constant input parameters with their values are shown. In addition, the cylinder had 0 °C initial uniform temperature T_i and at $t > 0$ the surface temperature T_s was maintained at 800 °C. Under such conditions, the temperature distribution in the cylinder as a function of position and time [11] is given by the following equation:

$$\frac{T(r,t)}{T_S} = 1 - 2\sum_{n=1}^{\infty} e^{-(k\beta_n^2 t)/(\rho c_p r_S^2)} \frac{J_0(r\beta_n / r_S)}{\beta_n J_1(\beta_n)} \tag{14}$$

Where

J_0 Bessel function of the first kind;
J_1 Bessel function of the second kind;
β_n $n = 1, 2, \ldots$ are the roots of $J_0(\beta) = 0$;
T_S Surface temperature;
r_S Cylinder radius;
r Radial coordinate;
k Thermal conductivity;
ρ Density;
c_p Heat capacity;
t Time.

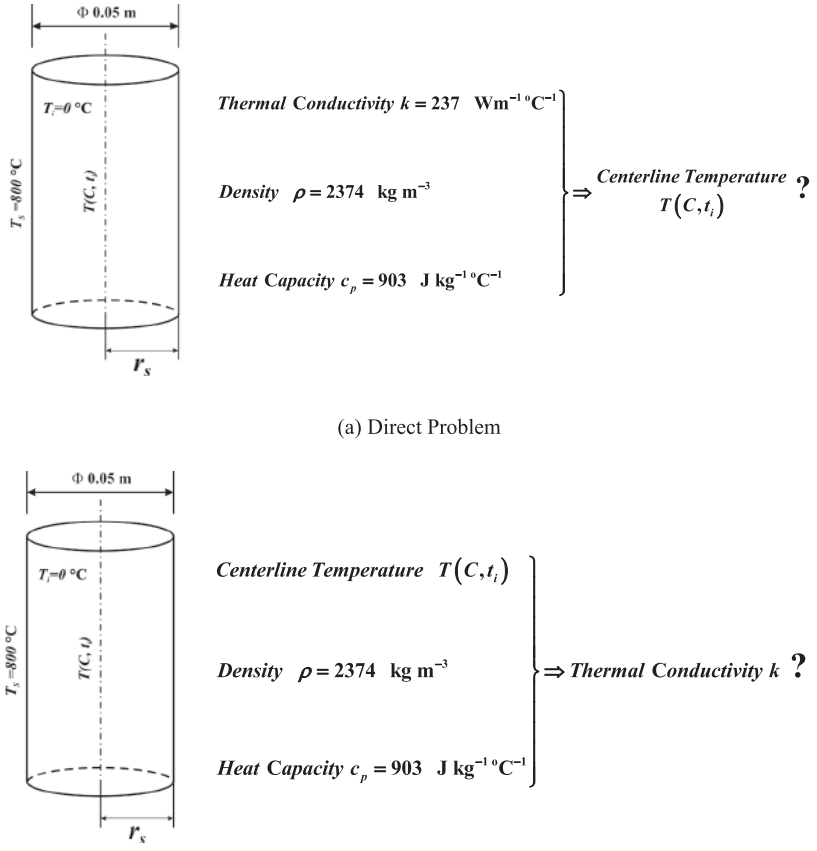

Fig. 10: Detail description of virtual experiment developed for validation of IHTP

The inverse problem was considered as shown in Figure 10 (b). In this case, the constant thermal conductivity of the cylinder is unknown, while all other quantities such as the constant boundary temperature, the initial temperature distribution, and the constant density and heat capacity of the cylinder are known. In addition, the compact centerline temperature $T(C, t_i)$ at different times t_i, which was calculated from Equation (14), was utilized as the reference temperature in the Inverse Heat Transfer Procedure. Then, the Inverse Heat Transfer Procedure was employed to estimate the unknown constant thermal conductivity of the cylinder. The results are represented in Figure 11. As can be seen from Figure 11, the estimated thermal conductivity of the cylinder agrees very well with the experimental one. The deviation observed, segment AB, between the estimated and actual one during the initial stage may be caused by the very small temperature gradient inside the cylinder during that stage. Furthermore, the compact centerline temperature, which was calculated with the IHTP code based on the estimated thermal conductivity, was compared with the analytical solution from Equation (14). It can be seen that both of them agree very well with each other. This fact lends more support that the IHTP developed to estimate thermal conductivity is valid.

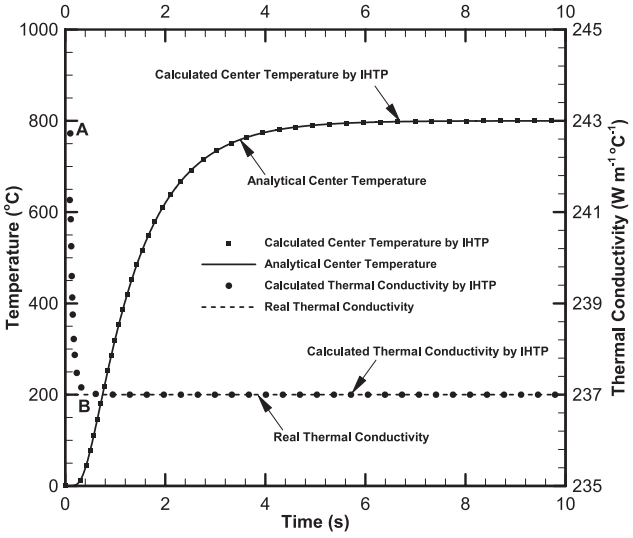

Fig. 11: Validation of IHTP code in a virtual experiment

5 Results and discussion

The estimated effective thermal conductivities of various Mn-Al compacts as well as the calculated compact centerline temperatures are shown in Figures 12 to 16. From these results, it was found that the effective thermal conductivities of various Mn-Al compacts were much lower than that of Al (237 W m^{-1} °C^{-1}), and close to that of Mn (7.8 W m^{-1} °C^{-1}). In addition, the dependence of the effective thermal conductivity of the Mn-Al compact on temperature was found to be very small in the temperature range examined (about 250~600 °C). Meanwhile, the calculated compact centerline temperature based on the estimated effective thermal conductivity agrees well with the one measured experimentally. This lends further support to the conclusion that the IHTP developed is well-grounded.

Table 3 lists the average compact effective thermal conductivities of various Mn-Al compacts estimated by IHTP as well as the measured compact porosities pre-

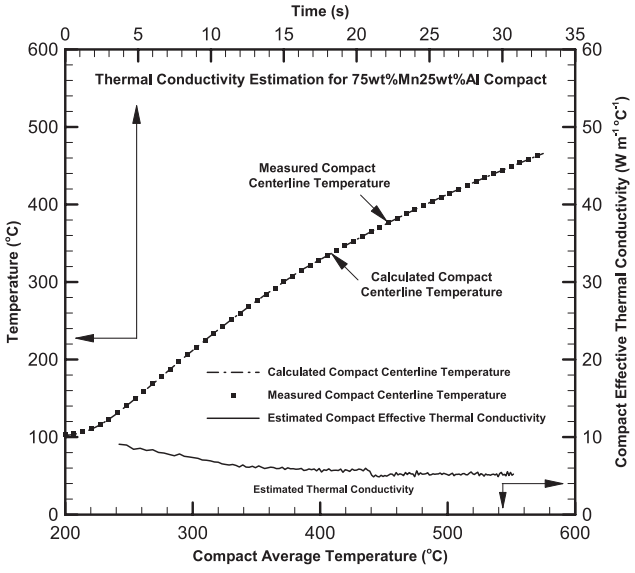

Fig. 12: Estimated Thermal Conductivity of a 75wt%Mn25wt%Al Compact

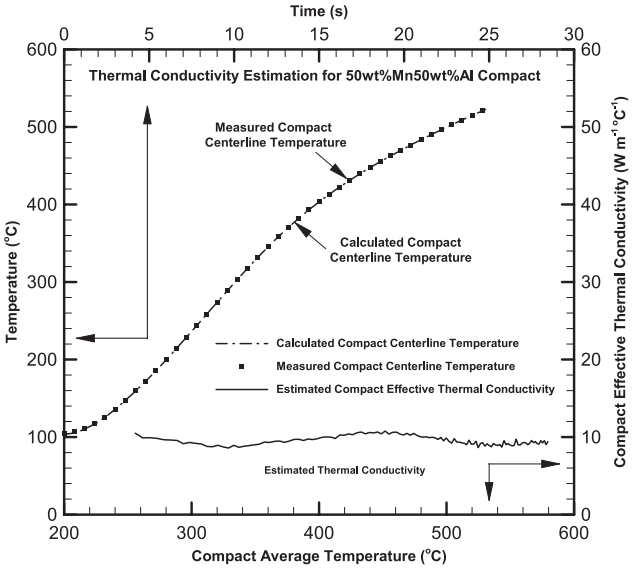

Fig. 14: Estimated Thermal Conductivity of a 50wt%Mn50wt%Al Compact

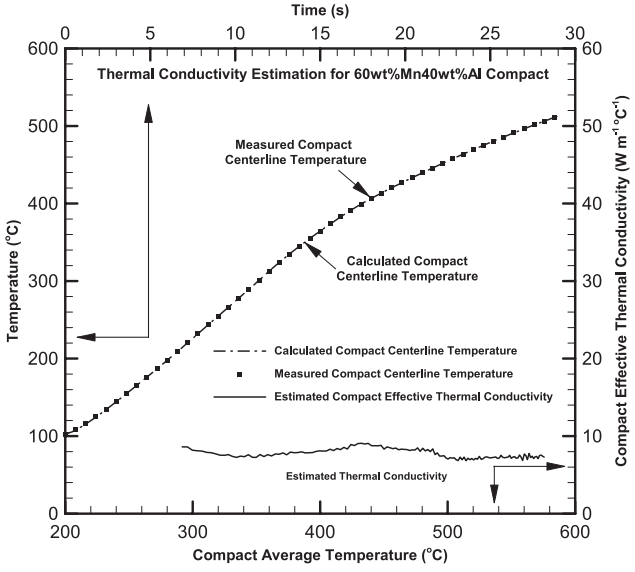

Fig. 13: Estimated Thermal Conductivity of a 60wt%Mn40wt%Al Compact

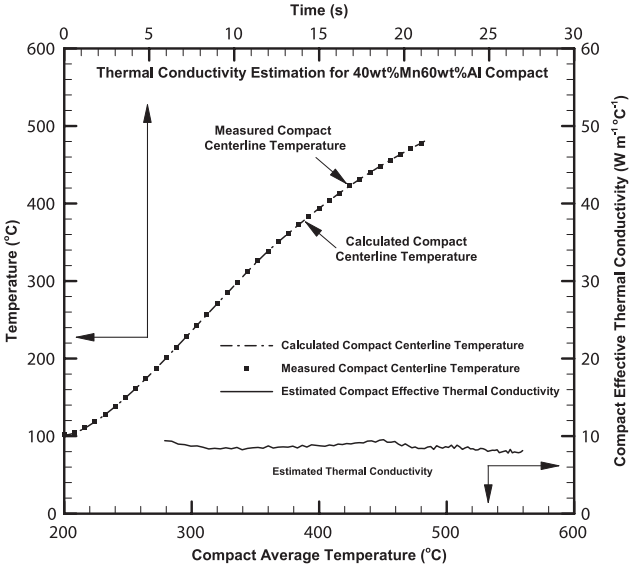

Fig. 15: Estimated Thermal Conductivity of a 40wt%Mn60wt%Al Compact

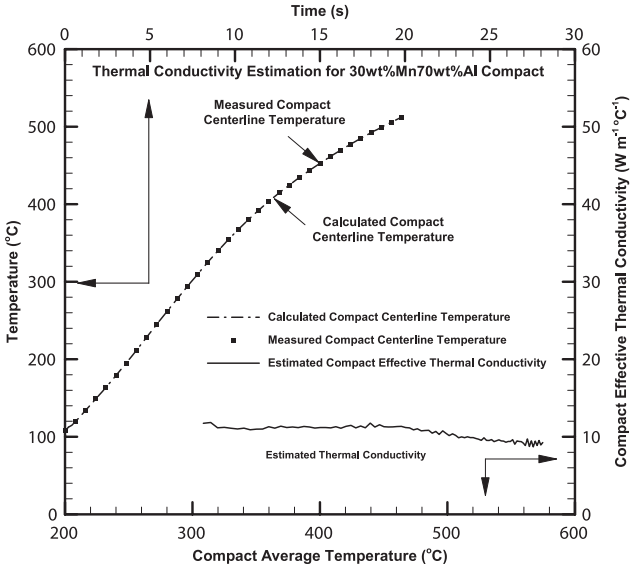

Fig. 16: Estimated Thermal Conductivity of a 30wt%Mn70wt%Al Compact

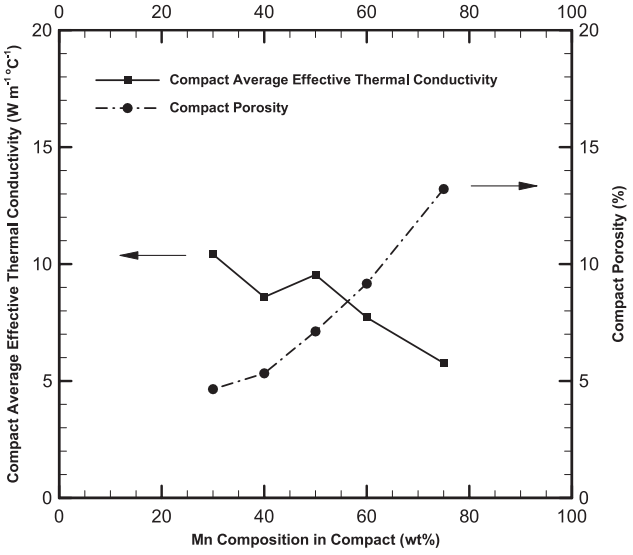

Fig. 17: Effect of Mn composition and porosity in Mn-Al compacts on effective thermal conductivity

Compact Type	Average Effective Thermal Conductivity (W m^{-1} °C^{-1})	Porosity [8] (%)
75wt%Mn25wt%Al	5.8	13.2
60wt%Mn40wt%Al	7.7	9.2
50wt%Mn50wt%Al	9.5	7.1
40wt%Mn60wt%Al	8.6	5.3
30wt%Mn70wt%Al	10.4	4.7

Table 3: Average effective thermal conductivities and porosities of various Mn-Al compacts

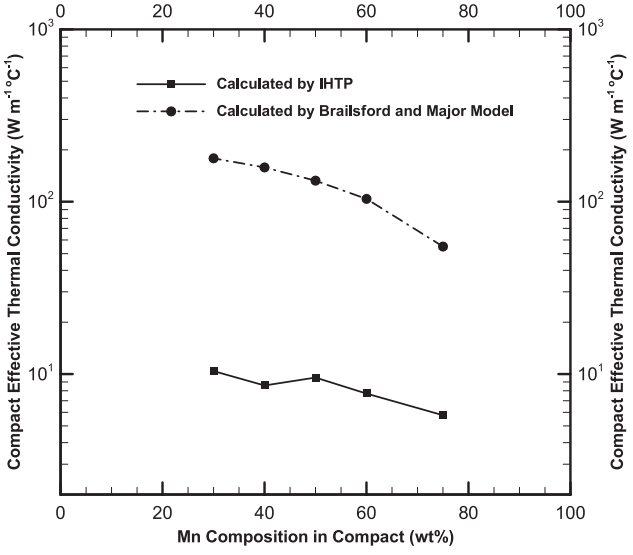

Fig. 18: Comparison between compact effective thermal conductivities estimated by IHTP and calculated by Brailsford and Major model [1]

sented in references [7, 8]. These data also are plotted in Figure 17. From these results, it seems that the effective thermal conductivities of various compacts decrease with an increase in Mn composition in the compact, and with an increase in porosity of the compact.

The theoretical effective thermal conductivities of various Mn-Al compacts have been calculated using the Brailsford and Major model [1]. The details of this calculation are represented in Appendix I. The comparison between the compact effective thermal conductivities estimated by IHTP and by the Brailsford and Major model [1] is displayed in Figure 18. It can be seen that there is a very large discrepancy between them. This result is not unexpected since many factors are posited to affect the compact effective thermal conductivity, as mentioned at the outset. It is impossible to include all factors into the theoretical model. In other words, the model does not necessarily fit the experimental conditions. When using the Brailsford and Major model to calculate the effective thermal conductivities of various Mn-Al compacts, three aspects may contribute to the large discrepancies. First, the Brailsford and Major model solves the thermal conductivity of randomly-sized spheres of one medium randomly distributed in another medium, but the shape of the Mn and Al particles used for manufacturing the Mn-Al compact is irregular, and as such, the particles cannot be

regarded as being spherical. Second, the presence of oxide layers of Mn and Al particles is not taken into account. The oxide layer will slow down the heat transfer between particles. Third, the thermal conductivity of very fine powders may be only a fraction of the values cited in the literature. Depending on the method of manufacture of the powders, the individual powder is in a stressed condition with a large number of defects, which lowers its thermal conductivity. A similar observation existed in the investigation by Gruzdev et al. [12]. With the aim of developing a method to predict the thermal conductivity of cold-pressed porous powder materials (CPPMs), the following conclusions were reached. The methods of calculating thermal conductivity on the basis of geometric modeling of the structure of pressed materials, were in close agreement with experimental results from (a) composite materials produced in dynamic pressing, (b) hot pressing, and (c) long time high temperature sintering. However, use of these methods for calculating the thermal conductivity of cold-pressed powder materials led to qualitative and substantial (up to 500%) quantitative discrepancies between calculated and experimental results. The Mn-Al powder compacts used in our experiments are cold-pressed powder materials. Therefore, in keeping with Gruzdev's findings [12], the large discrepancy observed in our study is not surprising.

6 Conclusions

An inverse heat transfer procedure was developed which estimates the effective thermal conductivity of Mn-Al compacts. The input of this procedure is the measured temperature histories at distinct locations of the compact. This procedure was validated with the help of a virtual experiment.

The estimated effective thermal conductivities of various Mn-Al compacts are in the range of 5.5 to 10.5 W m^{-1} °C^{-1}, which are much lower than that of Al (237 W m^{-1} °C^{-1}), and close to that of Mn (7.8 W m^{-1} °C^{-1}). The effective thermal conductivities of various Mn-Al powder compacts decrease with an increase in the compact's Mn composition and porosity. A purely theoretical prediction of Mn-Al compact thermal conductivity is substantially higher than the estimates of the IHTP, and as such would render a substantive error margin when applied to an industrial practice.

The dependence of the effective thermal conductivity of the Mn-Al compact on temperature is minimal in the examined temperature range from about 250 to 600 °C.

Nomenclature

English symbols

A_N	Interface area between control volume N and $N+1$, m^2
C_{N1}, C_{N2}	Constants in Equation (7)
c_P	Heat capacity, J kg^{-1} °C^{-1}
k	Thermal conductivity, W m^{-1} °C^{-1}
k_{Al}	Thermal conductivity of Al, W m^{-1} °C^{-1}
k_e	Estimated thermal conductivity, W m^{-1} °C^{-1}
k_{eff}	Effective thermal conductivity of the two phase assembly considering the existence of porosity, W m^{-1} °C^{-1};
k_{mix}	Thermal conductivity of the two phase assembly, W m^{-1} °C^{-1};
k_{Mn}	Thermal conductivity of Mn, W m^{-1} °C^{-1}
k_1	Thermal conductivity of the first phase, W m^{-1} °C^{-1};
k_2	Thermal conductivity of the second phase, W m^{-1} °C^{-1};
k_{g1}	First guessed compact thermal conductivity, W m^{-1} °C^{-1}
k_{g2}	Second guessed compact thermal conductivity, W m^{-1} °C^{-1}
N	Node number
r	Cylindrical coordinate in radial direction, m
r_S	Cylinder radius in Equation (14)
Δr	Mesh size, m
R_{Edge}	Distance from compact center to compact edge measurement point, m
t	Time, s
t_i	Time, s
t_{a1a2}	Starting time of IHTP
t_{b1b2}	Ending time of IHTP
Δt	Time step, s
T	Temperature, °C
$T(r,t)$	Cylinder temperature at radial coordinate r and time t
$T(C,t)$	Measured temperature at the center of the cylindrical compact, °C
$T(C,t_i)$	Measured temperature at the center of the cylindrical compact at time t_i, °C
$T(E,t)$	Measured temperature at the edge of the cylindrical compact, °C
T_N^P	Temperature of control volume N at time $P\Delta t$, °C
T_N^{P+1}	Temperature of control volume N at time $(P+1)\Delta t$, °C
$T_{1,g1}^{p+1}$	Calculated compact centerline temperature based on k_{g1} at $(P+1)\Delta t$, °C

$T_{1,g2}^{p+1}$ Calculated compact centerline temperature based on k_{g2} at $(P+1)\Delta t$, °C
T_i Initial temperature, °C
T_S Surface temperature, °C
V_{f1} Volume fraction of the first phase, %
V_N Volume of control volume N, m^3

Greek symbols

ρ Density, kg m^{-3}
ρ_{Al} Al density, g cm^{-3}
ρ_{Mn} Mn density, g cm^{-3}
ϕ Porosity of the two phase assembly, %.

Mathematical symbols

J_0 Bessel function of first kind
J_1 Bessel function of second kind
β_n $n = 1, 2, \ldots$ are the roots of $J_0(\beta) = 0$

Acknowledgments

The authors would like to recognize the financial contribution of the Natural Sciences and Engineering Research Council through a Strategic Grant.

Throughout the course of this investigation Mr. Timothy J. Kosto of Milward Alloys Inc, in Lockport NY, USA, was extremely generous with his time and with sharing the wealth of information he has accumulated over his extensive experience in industry. Without a doubt by tapping into his vast knowledge and experience and insights the authors benefitted greatly.

Received: May 17, 2012. Accepted: July 12, 2012.

References

[1] J. E. Parrot and A. D. Stuckes, "Thermal Conductivity of Solids", Pion Limited, London, 1975, pp. 132–133.
[2] S. Miura, Y. Terada, T. Suzuki, C. T. Liu, Y. Mishima, "Thermal Conductivity of Ni-Al Powder Compacts for Reaction Synthesis", Intermetallics, 8(2000), pp. 151–155.
[3] A. Kurt, H. Ates, "Effect of Porosity on Thermal Conductivity of Powder Metal Materials", Materials and Design, 28(2007), pp. 230–233.
[4] P. Grootenhuis, R. W. Powell and R. P. Tye, "Thermal and Electrical Conductivity of Porous Metals Made by Powder Metallurgy Methods", Proceedings of the Physical Society, Section B 65, 1952, pp. 502–511.
[5] K. Y. Sastry, L. Froyen, J. Vleugels, E. H. Bentefour, and C. Glorieux, "Effect of Porosity on Thermal Conductivity of Al-Si-Fe-X Alloy Powder Compacts", International Journal of Thermophysics, Vol. 25, No. 5, September 2004, pp. 1611–1621.
[6] A. I. Krivchikov, B. Ya. Gorodilov, and O. A. Korolyuk, "A Setup for Studying the Low-Temperature Thermal Conductivity of Powder Samples", Instruments and Experimental Techniques, Vol. 48, No. 3, 2005, pp. 417–421.
[7] T. J. Reinhart, "Engineered materials handbook", Metals Park, Ohio: ASM International, c1987, Volume 4, pp. 613.
[8] Z. Li and S. A. Argyropoulos, "The Assimilation of Mn-Al powder compacts in liquid Mg: Exothermicity and Recovery Issues", Canadian Metallurgical Quarterly, Vol. 48, No. 4, pp. 399–418, 2009.
[9] Z. Li and S. A. Argyropoulos, "The Assimilation Mechanism of Mn-Al Compacts in Liquid Mg", Materials Transactions of Japan Institute of Metals, Vol. 51, No. 8(2010) pp. 1371–1380.
[10] "McGraw-Hill dictionary of scientific and technical terms, 6th Edition" New York: McGraw-Hill, c2003, pp. 1415.
[11] H. S. Carslaw and J. C. Jaeger, "Conduction of Heat in Solids", Oxford Clarendon Press, 1959, pp. 199.
[12] V. A. Gruzdev, Yu. P. Zarichnyak, and Yu. A. Kovalenko, "Effect of Pressing Process Parameters on the Thermal Conductivity of Cold-Pressed Porous Powder Compact", Powder Metallurgy and Metal Ceramics, Vol. 28, No. 3, 1989, pp. 164–168.

Appendix I

In this section, the effective thermal conductivities of various Mn-Al compacts are calculated using the Brailsfold and Major model [1]. This model predicts the thermal conductivity for randomly-sized spheres of the first phase randomly distributed in the second phase. It covers the full range of composition, by regarding a random two-phase assembly composed of the two single phases in the correct proportions, embedded in a random mixture of the same two phases have a conductivity equal to the average value of the conductivity of the two-phase assembly. The thermal conductivity k_{mix} of such an assembly is given by

$$k_{mix} = \frac{k_2}{4}\left[(3V_{f1}-1)\frac{k_1}{k_2} + 2 - 3V_{f1} + \left\{\left[(3V_{f1}-1)\frac{k_1}{k_2} + 2 - 3V_{f1}\right]^2 + 8\frac{k_1}{k_2}\right\}^{1/2}\right] \quad \text{(I-1)}$$

Where

k_{mix} Thermal conductivity of the two phase assembly, W m^{-1} °C^{-1};
k_1 Thermal conductivity of the first phase, W m^{-1} °C^{-1};
k_2 Thermal conductivity of the second phase, W m^{-1} °C^{-1};
V_{f1} Volume fraction of the first phase, %.

Compact Type	Volume Fraction of Mn Component in Mn-Al Compact V_{f1} (%)	Compact Thermal Conductivity by Brailsford and Major Model k_{mix} (W m^{-1} °C^{-1})	Compact Porosity ϕ (%)	Effective Compact Thermal Conductivity k_{eff} (W m^{-1} °C^{-1})
75wt%Mn25wt%Al	52.2	67.5	13.2	54.9
60wt%Mn40wt%Al	35.3	119.5	9.2	103.8
50wt%Mn50wt%Al	26.7	147.7	7.1	132.5
40wt%Mn60wt%Al	19.5	171.4	5.3	158.1
30wt%Mn70wt%Al	13.5	191.6	4.7	178.5

Table I-1: Effective thermal conductivities of various Mn-Al compacts calculated using Brailsford and Major model [1]

It is worth noting that Equation (I-1) calculates the thermal conductivity of a two phase assembly without porosity. Considering the porosity in the assembly, the effective thermal conductivity k_{eff} can obtained through modifying k_{mix} with the following formula [1]

$$\frac{k_{eff}}{k_{mix}} = \frac{1-\phi}{1+\frac{1}{2}\phi} \tag{I-2}$$

Where

k_{eff} Effective thermal conductivity of the two phase assembly considering the existence of porosity, W m^{-1} °C^{-1};

ϕ Porosity of the two phase assembly, %.

Using Equations (I-1) and (I-2), the theoretical effective thermal conductivities of Mn-Al metal powder compacts with various compositions used in our experiments are calculated. The results are listed in Table I-1. Thermo-physical properties of Mn and Al used for this calculation are: $k_{Al} = 237$ W m^{-1} °C^{-1}, $k_{Mn} = 7.8$ W m^{-1} °C^{-1}, $\rho_{Al} = 2.7 \times 10^3$ kg m^{-3}, and $\rho_{Mn} = 7.43 \times 10^3$ kg m^{-3}.